# Effect of copper dispersion on SBA-15 and SBA-16 affinity towards carbon dioxide-an approach through thermal programmed desorption

Kawter Nor El Houda Sekkal, Rachida Ouargli-Saker, Asma Kawther Lachachi, Meriem Zekkari, Ana-Paola Beltrao-Nunes, Laure Michelin, Loïc Vidal, Bénédicte Lebeau, Abdelkrim Azzouz

# Effect of copper dispersion on SBA-15 and SBA-16 affinity towards carbon dioxide - An approach through thermal programmed desorption

**Kawter Nor El Houda Sekkal[1], Rachida Ouargli-Saker[1,2], Asma Kawther Lachachi[1,2], Meriem Zekkari[1,2], Ana-Paola Beltrao-Nunes[2,3], Laure Michelin[4,5], Loïc Vidal[4,5], Bénédicte Lebeau[4,5], Abdelkrim Azzouz[2,6*]**

*[1] Laboratoire des Sciences, Technologie et Génie des Procédés, Université des Sciences et de la Technologie d'Oran Mohamed Boudiaf, El M'naouer, BP 1505, Oran, Algérie.*
*[2] Nanoqam, Department of Chemistry, University of Quebec at Montreal, H3C3P8,Canada.*
*[3] LQAmb, Laboratório de Química Analítica Ambiental, Programa PG em Engenharia e Tecnologia de Materiais, Pontifícia Universidade Católica do Rio Grande do Sul, Brasil.*
*[4] Université de Haute Alsace (UHA), CNRS, IS2M UMR 7361, F-68100 Mulhouse, France.*
*[5] Université de Strasbourg, F-67000 Strasbourg, France.*
*[6] École de Technologie Supérieure, Montréal (Québec), Canada, H3C 1K.3*

** Corresponding author Email address: azzouz.a@uqam.ca*

**Abstract**

A new approach for the synthesis of zero-valent copper nanoparticles (CuNP) supported on ordered mesoporous silica SBA-15 and SBA-16 by using vegetal antioxidants, coffee Robusta and green tea was developed in the present work. Diverse characterization techniques such as X-ray diffraction, nitrogen adsorption–desorption, transmission electron microscopy, thermogravimetric analysis, Fourier transform infrared spectroscopy, and thermal programmed desorption of $CO_2$ and water allowed stating that the appreciable specific surface area and porosity favored CuNP formation. Copper-loaded SBA-15 and SBA-16 exhibited higher surface basicity and hydrophilic character according to the type of the source of reducing agents and silica framework, respectively. OH-compounds interactions with both CuNP and SBA surface and more particularly with available Si-O-Si groups were found to promote metal dispersion reducing the particle size. The results obtained herein open promising prospects for designing low cost and "green" silica-based materials with judiciously tailored basicity and hydrophilic character for catalysis, adsorption and other surface processes.

**Keywords:** SBA; Metal nanoparticles; Copper; Green tea; Coffee; $CO_2$.

## 1. Introduction

So far, the synthesis of ordered mesoporous materials of SBA-15 and SBA-16 is often justified by their beneficial adsorptive and catalytic properties for numerous purposes [1, 2] and more particularly for environmental applications [3, 4]. Their respective bi-dimensional hexagonal (P6mm) and tri-dimensional cubic symmetry (Im3m) [5, 6] confer them organized and regular porosity with high specific surface area and large mesopores. These features allow incorporating diverse chemical species for potential adsorption and catalysis purposes [7]. Notwithstanding that a wide literature considers SBA-like silica as being neutral materials, the mere presence of silanol groups can induce diverse interactions with species in aqueous media [8-11]. These interactions range from purely physical sorption to chemical reactivity [2]. Owing to some of these interactions, SBA materials can act as host matrices for metal nanoparticles (MNP) [12, 13].

The expanded frameworks of SBAs and their intrinsic surface properties allow achieving suitable modifications according to the targeted applications. Once loaded with metal particles or ions, such materials can acquire interesting surface properties as catalysts [14-16], adsorbents for pollutants [17], materials for medicine [18-20], matrices for hydrogen storage [21, 22] and sensors/components in electronics [23, 24]. Metal-zero incorporation is one of many other strategies to promote Lewis basicity and modify the hydrophilic character of SBA-15 and SBA-16 materials for tailoring their surface affinity towards acidic gas and water. This is the main objective of the present work.

Currently, the most common methods for preparing zero-valent metals (ZVM) use toxic and harmful chemical reducers such as sodium borohydride ($NaBH_4$) [25, 26], hydrazine ($N_2H_4$) [27], ethylene glycol [28] and volatile organic solvents such as toluene or chloroform [29]. There exists a wide variety of other compounds such as hydrogen, carbon monoxide and others that can behave more or less successfully as reducing agents, but some of them impose severe safety constraints and specific equipment requirements.

Successful results were obtained in previous works with sodium borohydride [12, 13, 30, 31], affording MNP incorporation inside the channels of mesoporous SBA- 15 and SBA-16 materials. The use of harmless and eco-friendly “green” reducing agent such as those provided by plants would be a judicious route to be explored. The chemical compositions of many plants include anti-oxidizing agents [32-34], some of them have already been investigated for a potential valorization of this property in the biosynthesis of metal nanoparticles [25, 32, 34-38]. Silver nanoparticles have been biosynthesized using an aqueous extract of green tea and other plants as reducing agents for biomedical use, environmental antifungal and other purposes [39-45]. Also, the $NaBH_4$ substitution by a green tea or coffee extracts well-known to display anti-oxidizing properties appears as an interesting challenge to be tackled. That is what motivated the use of tea and coffee in this work.

Tea and coffee extracts in water are regarded as dietary sources of anti-oxidizing agents often recommended for human health against oxidative stress [46] with growing interest for food, pharmacological and cosmetic applications [47]. Coffee contains more caffeine (methylxanthine) than tea (called theine in tea). However, their anti-oxidizing capacity is not due to caffeine but rather to 1,3,7-Trimethyl-1H-purine-2,6(3H,7H)-dione or 3,7-Dihydro-1,3,7-trimethyl-1H-purine-2,6-dione. This molecule differs from other antioxidizing compounds such as polyphenolic components such as epicatechin, epicatechin-3-gallate, epigallocatechin and epigallocatechin-3-gallate [48, 49]. These compounds belong to the so-called Chlorogenic acid (CGA) family, and paradoxically do not contain chlorine [50]. CGA was already reported to exhibit reducing properties in the synthesis of ZVM [51].

The types and chemical composition of polyphenols differ in coffee and tea, inasmuch as coffee is rich in phenolic acids, while tea is rich in flavonoids [52]. The reducing properties of phenolic compounds arise from their great capacity to be oxidized, playing a key role as antioxidants in living organisms. In green tea, epigallocatechin gallate appears as the main reducing agent, and the amount of phenolic components was found to decrease upon water heating up to the boiling point [53]. Additional beneficial effects of coffee and green tea reside in their contributions as encapsulating agents that prevents instant aggregation into bulkier clusters.

In the present work, the effect of coffee and green tea in the synthesis of copper nanoparticles in two ordered mesoporous silica matrices (SBA-15 and SBA-16) will be comparatively examined. Emphasis was made on a judicious approach that consists in providing evidence of the occurrence of Cu:O-matrix interactions on the basis of measurements using thermal programmed desorption of water and carbon dioxide. This new approach is quite original, more particularly when the adsorptive properties are correlated with structural and textural features of the synthesized metal-loaded organo-SBA samples. This is expected to provide valuable data on the affinity for carbon dioxide and water.

## 2. Experimental

### *2.1. SBA-like silica preparation*

In a first step, SBA-like silicas were prepared according to a previously reported procedure [1] by hydrothermal synthesis method in the following gels compositions: ***i.*** for SBA-15: 1 $SiO_2$: 0.059 P123: 56.13 HCl: 607.638 $H_2O$, and ***ii.*** for SBA-16: 1 $SiO_2$: 0.006 P123: 0.013 F127: 42.439 HCl: 442.876 $H_2O$. For this purpose, non-ionic surfactant Pluronic F127 block-copolymer (Aldrich) and/or Pluronic P123 block-copolymer, (MW = 5800, Sigma–Aldrich) were dissolved in deionized water and hydrochloric acid (37 %, Fluka) solution at 27 °C. Further, a specific amount of tetraethyl orthosilicate (TEOS, Aldrich) was added dropwise into the P123 solution and stirred at 37 °C for 20 h (**Scheme 1**). The resulting hydrogels were transferred into a teflon-lined stainless-steel autoclave

and maintained at 100 °C for 48 h. The white powders obtained were repeatedly washed with deionized water, filtered, then dried at 60 °C overnight and finally calcined at 550 °C for 6 h under airflow to remove the organic template.

### *2.2. Metal dispersion*

In a second step, copper-zero nanoparticles (CuNP) were synthesized by dispersing 0.5 g of calcined SBA-15 or SBA-16 samples in 50 mL of an aqueous infusion of 2 g Robusta coffee (Originating from Uganda and imported in Algeria from Sopex Group London Ltd) in 100 mL water previously boiled for 10 min and 5 mL of an aqueous solution of copper nitrate (1M) under stirring for 6 hours. Metal cation reduction was performed under $O_2$-free nitrogen stream. The resulting copper-loaded organo-SBA samples denoted as Cu/SBA-15-Coffee and Cu/SBA-16-Coffee, respectively were recovered through filtration and dried at 60 °C overnight. Similar procedures were employed using an aqueous solution of EL MARWAN green tea (imported in Algeria from China) for the preparation of their counterparts designated by Cu/SBA-15-Tea and Cu/SBA-16-Tea but under stirring for 17 hours (**Scheme 1**).

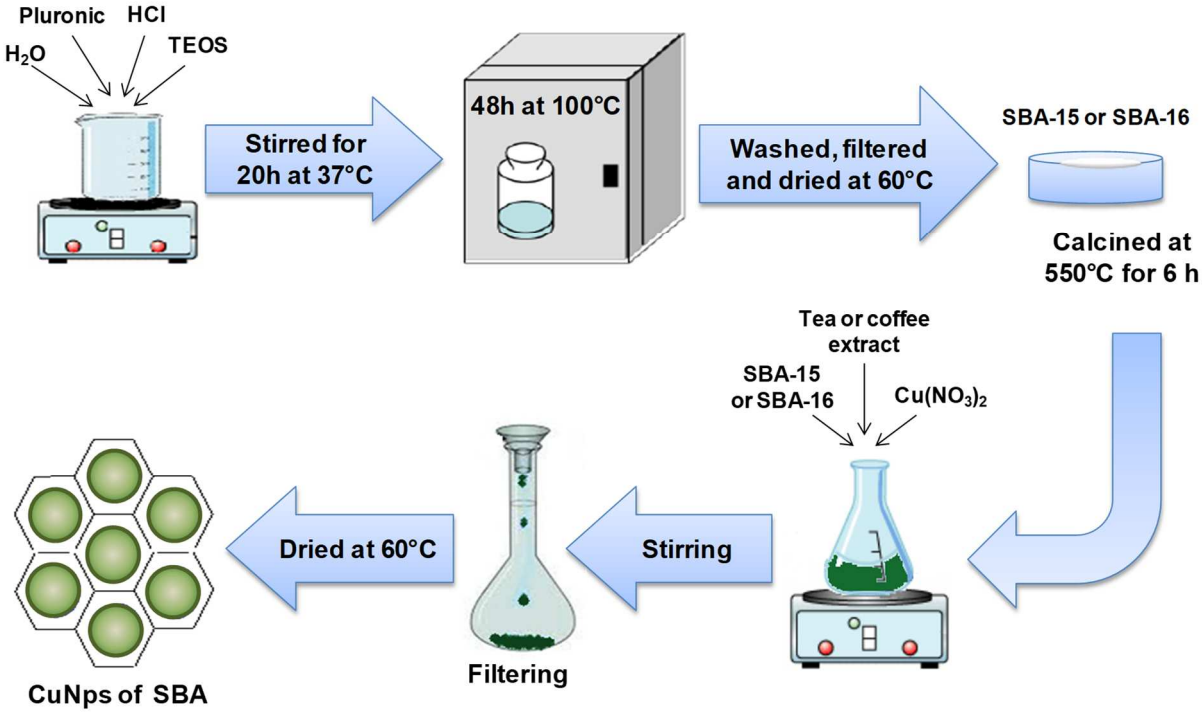


**Scheme. 1** Illustration of the different steps of the protocol for the synthesis of SBA-supported copper nanoparticles and characterization

The global chemical compositions of both aqueous extracts obtained by infusing similar amount

of roasted Coffee Robusta and Green-tea in boiled distilled water were assessed through reversed-phase high performance liquid chromatography but under different operating conditions as reported elsewhere [54]. For this purpose, one used an Alliance instrument and a hydrophobic C18 column (Agilent Eclipse Plus, 3.5 µm, 4.6 mm × 250 mm) coupled to a UV-detector (WATERS-2487 dual λ absorbance). The flow rate of the mobile phase (0,06 mL trifluoroacetic acid, TFA per 1 liter nanopure water) was set at a constant 1mL.min$^{-1}$ value (isocratic mod) with a 3µL injected volume. The data were treated by STAR acquisition software. Such a procedure allowed acquiring highly resolved peak for caffeine and chlorogenic acids (CGA).

The total amount of CGA for fully roasted Robusta beans is of ca. 3.95 g/kg dry sample, and accounts for approximately 5-6% of that of green Robusta beans. This marked CGA depletion upon roasting is due to CGA conversion into CGA-Lactones derivatives, and is in the range reported by the literature [54]. The total amount of catechins was of 28-31-%, depending on the age of the sample (1-3 years). The content of the main flavonoids involved in ZVM synthesis such as epigallocatechin gallate (EGCG), epicatechin 3-gallate (EGC), epigallocatechin (ECG), epicatechin (EC) and catechin (C) was of 0.82 g/kg in agreement with other works [55].

### *2.2. Characterization*

The synthesized materials were characterized by powder X-ray diffraction (XRD) using a PANalytical X'Pert Pro diffractometer with a Cu anode operating at 50 kV/40 mA (λ = 0.15418 Å) and Fourier transform infrared spectroscopy (DRIFTS, Nicolet 6700 FT-IR spectrometer, KBr pills, average IR scans = 64, resolution = 4 cm$^{-1}$). Deeper insights in copper dispersion on SBA materials were achieved through transmission electron microscopy (TEM) using a JEOL ARM200-CFEG microscope operating at 200 kV equipped with an Energy-dispersion X-ray fluorescence (ED-XRF) device. For TEM observations, few drops of high dispersed suspension previously ultrasonicated in chloroform were deposited on Au grid covered by Formvar/amorphous carbon film.

The specific surface area (SSA) and porosity were assessed from nitrogen adsorption-desorption isotherms recorded at -196 °C using a Micrometrics Tristar instrument. The samples were previously out-gassed overnight under vacuum at 70 °C. The SSA was determined using the Brunauer – Emmett – Teller method (BET) in the relative pressure range of 0.05 to 0.35. The average pore diameter was measured using the Barrett Joyner Halenda (BJH) model applied to the desorption branch. The microporous volume was evaluated using the *t*-plot method.

Thermal gravimetric analysis (TGA) was performed using a METTLER TOLEDO STAR apparatus, under airflow and a 5 °C.min$^{-1}$ heating rate from 30 to 800 °C. TGA measurements allowed establishing the thermal stability at temperature not exceeding 150 °C for accurate assessment of the surface basicity and hydrophilic character. These properties were expressed in terms of $CO_2$ and water

retention capacities (CRC and WRC, respectively) as estimated by thermal programmed desorption measurements (TPD) of $CO_2$ and water. TPD runs were achieved in a tubular glass reactor coupled to a Li-840A $CO_2$/ $H_2O$ dual Gas Analyzer. Each sample (40 mg, particle size of 0.05-0.1 mm) was previously contacted for ca. 40 min with dry $CO_2$ (1.5–500 mL) at 20 °C, under a nitrogen stream (15 $mL.min^{-1}$). After saturation, the non-adsorbed $CO_2$ excess was purged under similar gas stream until no $CO_2$ was detected. The CRC and WRC were measured at a 5 $mL.min^{-1}$ nitrogen stream at a 5 $°C.min^{-1}$ heating rate between 20 °C and 150 °C for repetitive TPD runs (TPD1, TPD2 and TPD3). This range was established according to the thermal stability of the materials as estimated by TGA measurements. Purely qualitative TPD analysis was also achieved through a non-repetitive TPD run up to 150 °C and even higher temperatures for Cu-loaded matrices with residual polycondensed hydrocarbons.

## 3. Results and discussion

### *3.1. Structural features*

SBA-15, Cu/SBA-15-Coffee and Cu/SBA-15-Tea displayed almost similar XRD patterns with a prominent peak (100 plane family) at 2θ ca. 1.02° and two peaks at 2θ ca. 1.68 and 1.92° assigned to the (110) and (200) planes, respectively [6, 56] (**Fig. 1a**). Assessment of the unit cell dimension, defined as $a_0=d_{100}$ $(2/3^{1/2})$, gave a value of 10 nm, which is typical of a P6mm hexagonal symmetry.

The corresponding d-spacings were assessed as being of 8.66 nm (100), 5.3 nm (110) and 4.6 nm (200), respectively. Noticeable attenuation in peak intensity was observed for Cu/SBA-15-tea, but much less pronounced for Cu/SBA-15-coffee. This must be due to slight framework distortions due to the formation of organic flavonoids or polyphenol clusters with MNPs, respectively, within the mesoporous channels [52]. SBA-16, Cu/SBA-16-Coffee and Cu/SBA-16-Tea showed XRD patterns with a prominent 100 XRD line at 2θ = 0.9° but barely observable 110, 200 and 211 reflections (**Fig. 1b**). This is a special feature of a highly uniform 3D cubic cage structure (Im3m space group structure) [57]. Calculations gave a d-spacing (110) of 9.8 nm and a unit cell dimension of 13.85 nm.

Extended XRD patterns up to 70 degrees only revealed apparently flat base line, due to the low amounts of incorporated copper. Barely detectable XRD lines at 2-Theta values of 43-44 degrees (111 plane family) and 50.5 degrees (220 plane family) provides evidence of the occurrence of $Cu^0$ at least. This low XRD sensitivity for such materials suggests a high metal dispersion into fine metal particles. ED-XRF measurements gave CuO ($Cu^0$) contents below the XRD technique sensitivity, as this will be examined further.

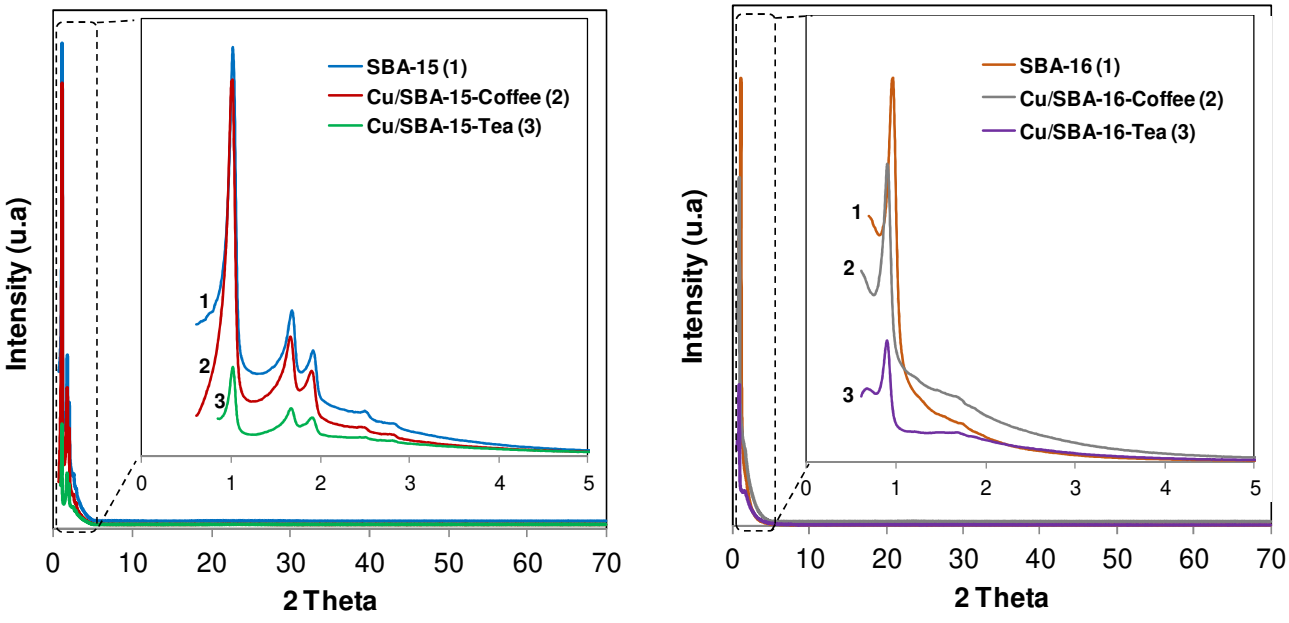


*a* *b*

**Fig. 1** Small and large angle XRD patterns for SBA-15 and Cu/SBA-15 (**a**) and SBA-16 and Cu/SBA-16 (**b**).

The same sequence in peak intensity depletion was noticed after CuNP incorporation. Different binary and even ternary interactions must be involved between metals, SBA surfaces and organic components. Such interactions should lead to more or less compacted metal-organic clusters and more or less spread throughout the entire silica surfaces. Deeper insights were achieved by an accurate assessment of the textural and surface properties of the materials.

### *3.2. Textural properties*

Nitrogen adsorption/desorption isotherms gave slightly higher specific surface area of 656 $m^2.g^{-1}$ for SBA-16 in agreement the slightly higher d-spacings (110) and unit cell dimension as compared to SBA-15 (626 $m^2.g^{-1}$). These isotherms were found to be of type IV with a clear H1 type hysteresis loop for SBA-15 (**Fig. 2a**) and H2 type hysteresis loop for SBA-16 (**Fig. 3a**). Both isotherm types characterizes regular mesoporous channels [58] and specifically a uniform structure with cubic cage-type and cross-connected pores for SBA-16 [59]. SBA-15 displayed an average pore size around 68 Å (**Fig. 2b**), in agreement with the literature [60]. SBA-16 showed a much uniform structure with a narrower pore size range of 40 Å (**Fig. 3b**).

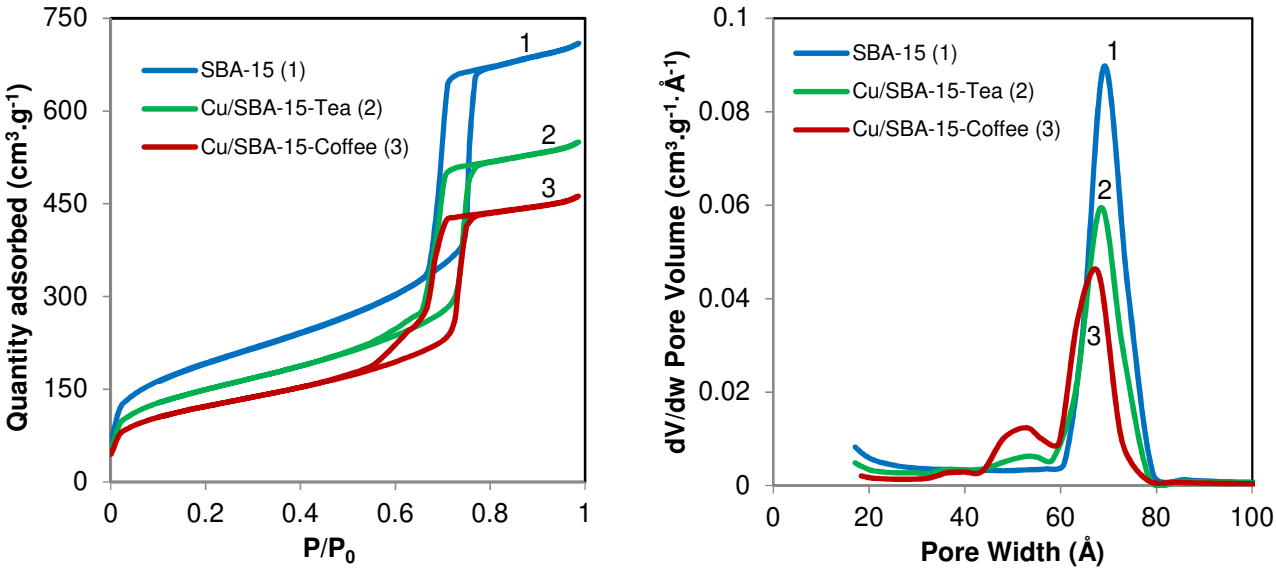


**Fig. 2** $N_2$ adsorption/desorption isotherms (**a**) and pore size distribution (**b**) of SBA-15 and its modified counterparts

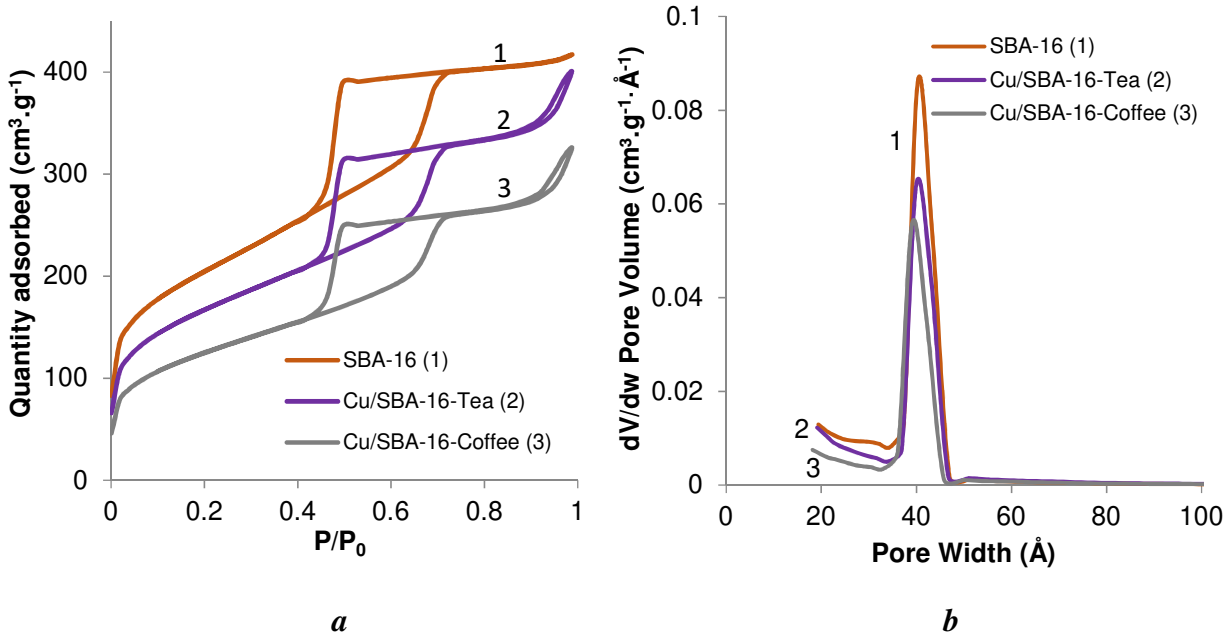


**Fig. 3** $N_2$ adsorption/desorption isotherms (**a**) and pore size distribution (**b**) of SBA-16 and its modified counterparts

This suggests a higher SSA but lower porosity for SBA-16 as compared to SBA-15 in agreement with our previous statement. Slight decreases in the textural properties were registered for both SBA materials after CuNP incorporation using both reducing agents. This was reflected by SSA decay upon CuNP insertion from 626 $m^2.g^{-1}$ for SBA-15 and from 656 $m^2.g^{-1}$ for SBA-16 down to 395 and 402 $m^2.g^{-1}$, respectively when using coffee as reducing agent (**Table 1**).

**Table 1** Textural properties of SBA samples and Cu-loaded counterparts

| Sample | $S_{BET}$ $(m^2.g^{-1})^a$ | Pore volume $(cm^3.g^{-1})^b$ | D $(nm)^c$ | Twall $(nm)^d$ | Dehydration mass loss %)[e] |
|---|---|---|---|---|---|
| SBA-15 | 626 | 1.001 | 6.9 | 3.1 | 8.3 |
| Cu/SBA-15-Coffee | 395 | 0.638 | 6.8 | 3.2 | 6.8 |
| Cu/SBA-15-Tea | 483 | 0.761 | 6.8 | 3.2 | 6.5 |
| SBA-16 | 656 | 0.581 | 4.0 | 8.0 | 6.0 |
| Cu/SBA-16-Coffee | 402 | 0.384 | 3.9 | 8.0.5 | 8.2 |
| Cu/SBA-16-Tea | 535 | 0.484 | 4.0 | 8.0 | 8.5 (Double step) |

[a] Specific surface area as assessed using BET model.
[b] Total pore volume estimated at $P/P_0 = 0.99$.
[c] Pore diameter estimated from adsorption branch using BJH model.
[d] The wall thickness was calculated using the following equations:
$T_{wall} = a_0$ – Pore size (BJH) for SBA-15 and $T_{wall} = (\sqrt{3}/2)a_0$ – Pore size (BJH) for SBA-16.
[e] This mass loss was the first step in the TGA diagram, and was assessed for temperatures not exceeding 150 °C.

Using green tea resulted in similar decay down to 483 for SBA-15 and to 535 $m^2.g^{-1}$ for SBA-16. This was accompanied by decreases in pore volume for both SBA materials upon CuNP incorporation. Here, the constant shape of the hysteresis loops is a precise indicator of copper dispersion within mesopores at least for Cu/SBA-15 samples. The slight increase of the wall thickness from 3.1 nm to 3.2 nm accounts the formation for ca. 0.1 nm layer of coffee and green-tea components inside SBA-15 channels. This phenomenon appears less pronounced in SBA-16, most likely due to the lower channel size that is expected to hinder the internal diffusion of the organic components of coffee and green-tea.

### *3.3. Particle size*

This was supported by TEM images, which revealed almost perfectly aligned CuNP with sizes mostly ranging from 2 to 6-7 nm, as statistically assessed between the smallest and largest black stain sizes measured graphically in a scale using Image-J software (**Fig. 4**). Such estimation is purely qualitative but quite satisfactory for mere comparison. The estimated particle size did not exceed the diameter of the channels as confirmed by the total absence of blackish stains on the external surface of both Cu/SBA-15-Coffee (**Fig. 4a**) and Cu/SBA-15-tea crystallites (**Fig. 4b**).

A random dispersion of much bulkier and more diffuse dark stains of ca. 20-30 nm was noticed on Cu/SBA-16-coffee (**Fig. 5a**) and smaller ones (10-20 nm) on Cu/SBA-16-tea (**Fig. 5b**). This suggests the formation of diffuse organic clusters entrapping finer Cups outside the SBA-16 channels. Such bulky clusters are expected to obstruct the channel entries and hinder the diffusion of organic molecules. Here, also green-tea components appear to promote higher copper dispersion and stabilization, presumably due to a higher chelating capacity.

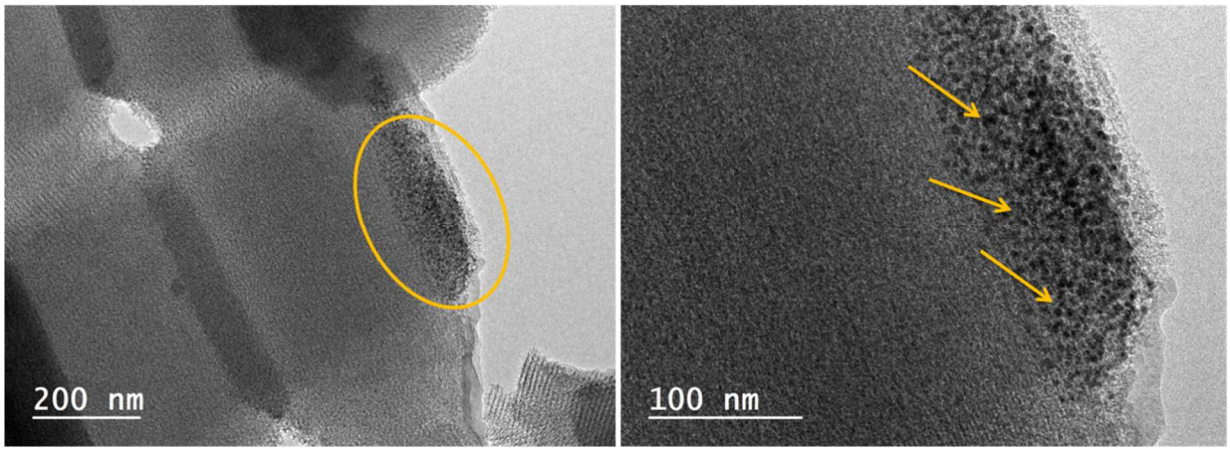


*a*

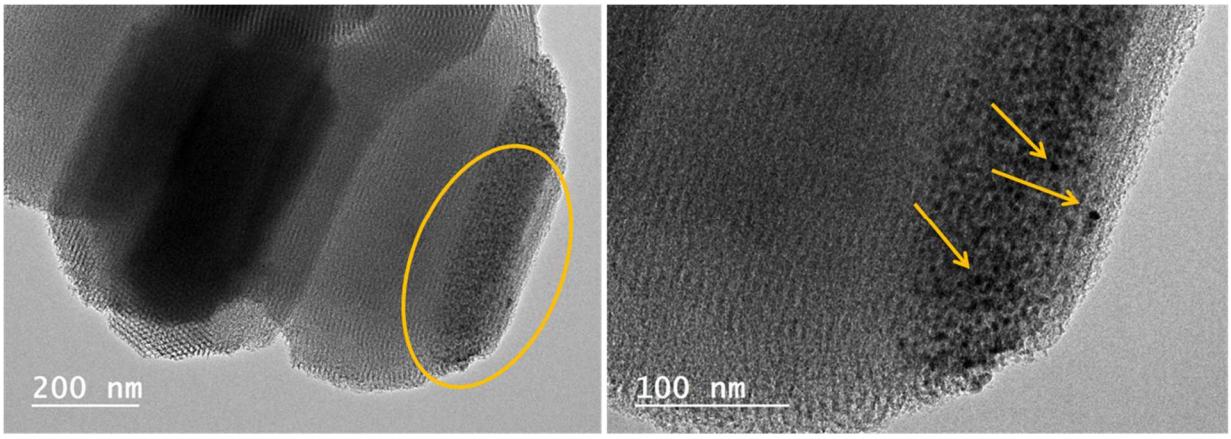


*b*

**Fig. 4** TEM images of Cu/SBA-15-Coffee (**a**) and Cu/SBA-15-Tea (**b**)

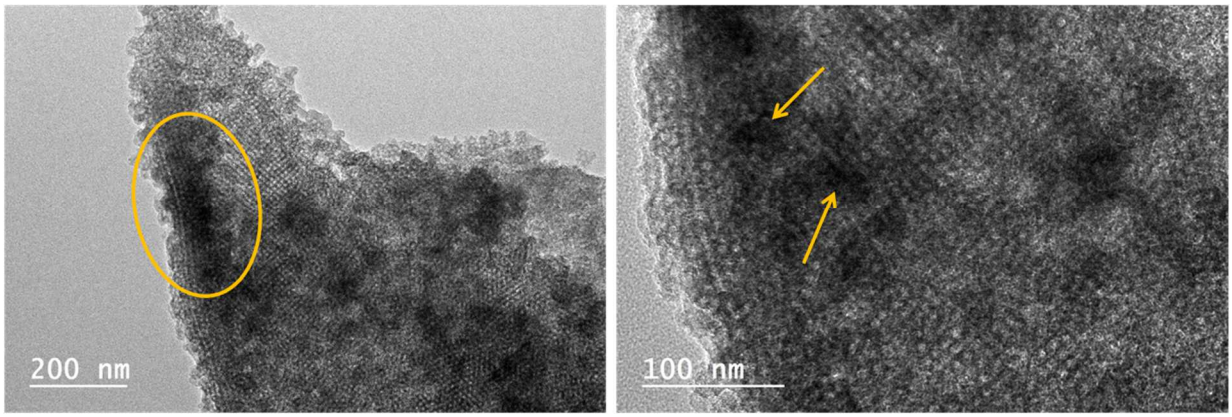


*a*

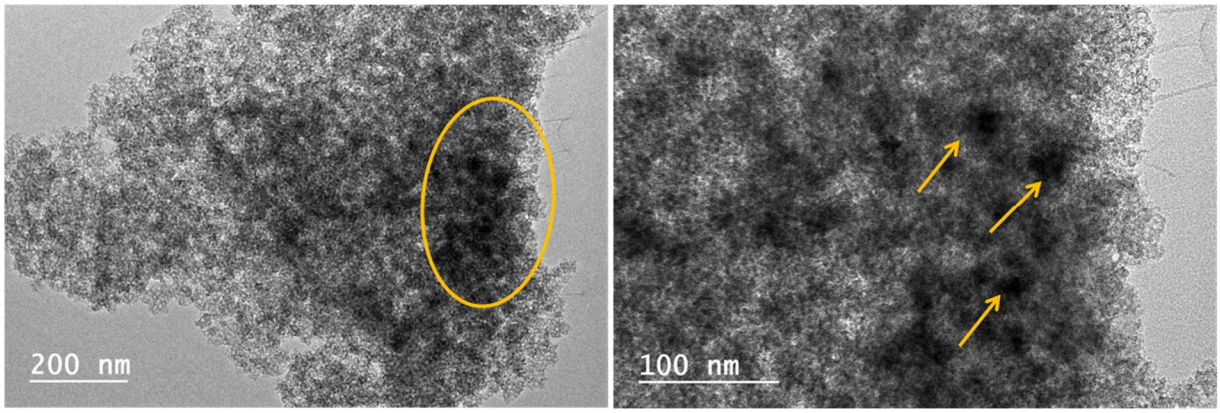


***b***

**Fig. 5** TEM images of Cu/SBA-16-Coffee (**a**) and Cu/SBA-16-Tea (**b**)

Deeper insights through ED-XRF analysis of some spots focused on the dark stains of both TEM images revealed ED-XRF signals of higher intensity at ca. 0.8-0.95 keV (Cu-$L_{alpha}$), 8.1-8.2 keV (Cu-$K_{alpha}$) and 8.8-8.9 keV (Cu-$K_{beta}$) in SBA-15 (**Fig. 6**) as compared to their SBA-16 counterparts (**Fig. 7**). This accounts for higher amounts (2.1 %) of incorporated copper in SBA-15 based samples. This cannot be explained by their close SSA values (626 versus 656 $m^2.g^{-1}$) but rather by the parallel channels of SBA-15 that promotes easier metal diffusion compared to SBA-16 (0.9% of incorporated copper).

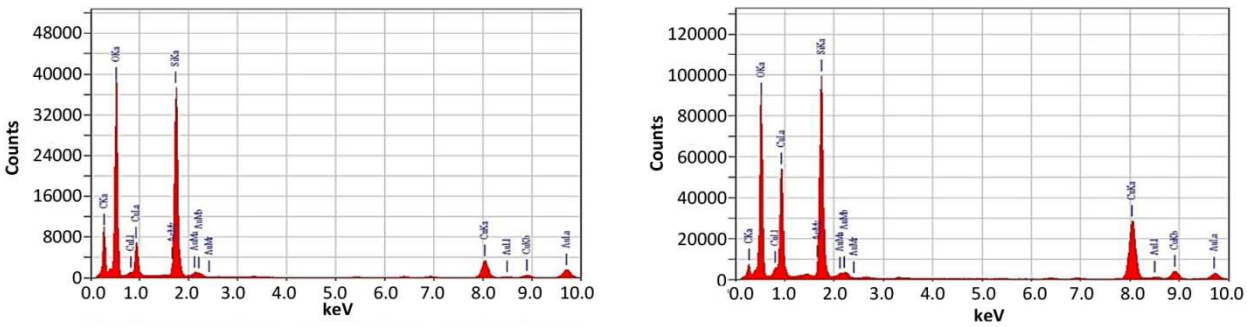


***a*** ***b***

**Fig. 6** ED-XRF analysis of Cu/SBA-15-Coffee (**a**) and Cu/SBA-15-Tea (**b**)

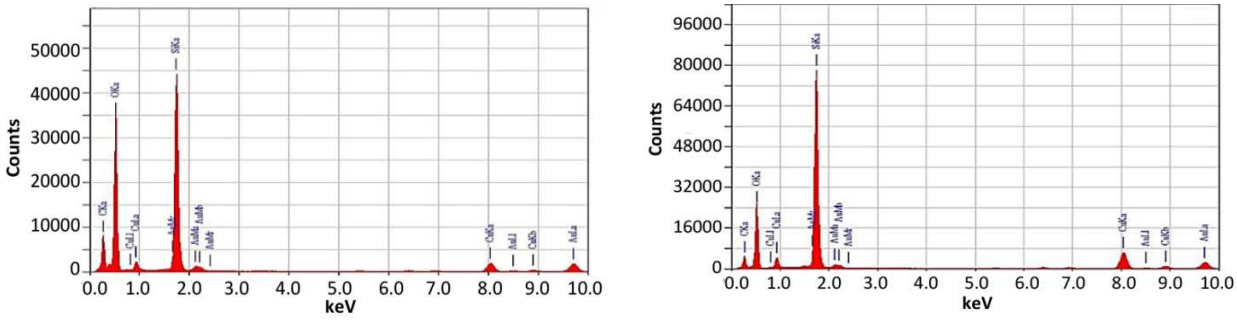


***a*** ***b***

**Fig. 7** ED-XRF analysis of Cu/SBA-16-Coffee (**a**) and Cu/SBA-16-Tea (**b**)

The more intense $K_{alpha}$ ray of carbon at ca 0.15-0.24 keV observed for Cu/SBA-15-Coffee (**Fig. 6a** and **Fig. 7a**) suggests the incorporation of higher amounts of coffee components as compared to tea-treated SBA samples (**Fig. 6b** and **Fig. 7b**). Nevertheless, this contrasts with the more intense $K_{alpha}$ ray of carbon noticed for Cu/SBA-15-Tea. ED-XRF measurements gave CuO ($Cu^0$) contents of 3.636 (2.9) % for Cu/SBA-15-Coffee, 3.571 (2.85) % for Cu/SBA-15-tea, 4.094 % (3.27) for Cu/SBA-16-Coffee and 1.907 (1.52) % for Cu/SBA-16-Tea. $Cu^0$ proportion of respectively 79.6, 79.8, 79.9 and 79.7 % of the total amount of copper species incorporated. Calculations based ED-XRF-based chemical compositions gave Copper/Carbon atomic ratio of ca. 0.26 for Cu/SBA-15-Coffee and of ca. 0.32 for Cu/SBA-15-Te.In other words, less tea components can disperse and stabilize more CuNP in SBA-15. Unlike polyphenolic acids in coffee, tea flavonoids are supposed to have more hydroxyls groups that act as effective chelating sites. A reverse sequence was observed for Cu/SBA-16, presumably due to the low contribution of the internal surface.

These amounts of CuNP are fairly appreciable compared to those reported a wide variety of works. They mainly arise from: ***i.*** a reduction process performed under $O_2$-free nitrogen stream to avoid metal re-oxidation and ***ii.*** The in-situ presence of coffee and green-tea extract that insures quick CuNP entrapment and protection against re-oxidation. Structure compaction around CuNP is a key factor in this regard.

### *3.4. Thermal behavior and changes in hydrophilic character*

TGA analysis (**Fig. 8**) showed higher weight loss of ca. 8.2-8.3 % for SBA-15 between 20 and 150 °C as compared to that of SBA-16 (6.0 %). These values were attributed to reversible dehydration and indicates higher moisture content in SBA-15 most likely due to its larger pore volume (1.001 $cc.g^{-1}$ versus 0.58 $cc.g^{-1}$) and diameter (6.9 versus 4.0 nm) (**Table 1**). This higher porosity of SBA-15 mainly arises from its thinner pore wall (3.1 nm) as compared to that of SBA-16 (8.0 nm). The much weaker mass loss noticed beyond 150 °C up to 700 °C was attributed to dehydroxylation [1].

Marked changes in the TGA patterns of were registered upon CuNP incorporation. This was reflected by lower moisture content for both modified SBA-15 samples (6.2-6.5 %). This visible decay in hydrophilic character must be due to a partial coverage of the silica surface by organic species. The reverse phenomenon was observed for modified SBA-15 samples with an improvement of the moisture content up to 8.2-8.3 %. This is not related to the textural properties, since the pore volume and diameter remains almost constant around 3.9-4.0 nm and 8.0-8.1 nm, respectively. The most plausible explanation resides in the occurrence of ternary [Organic hydroxyl:Metal:Water] interaction. In others words, the mere presence of OH groups belonging to polyphenolics acids and oxidized flavonoids around MNP enhances the surface affinity towards water [61]. This phenomenon

seems to be more pronounced in diffuse 3D Cu-loaded organic clusters on the external surface than in confined surrounding with limited surface for 2D [Silanol:Metal:Water] interaction.

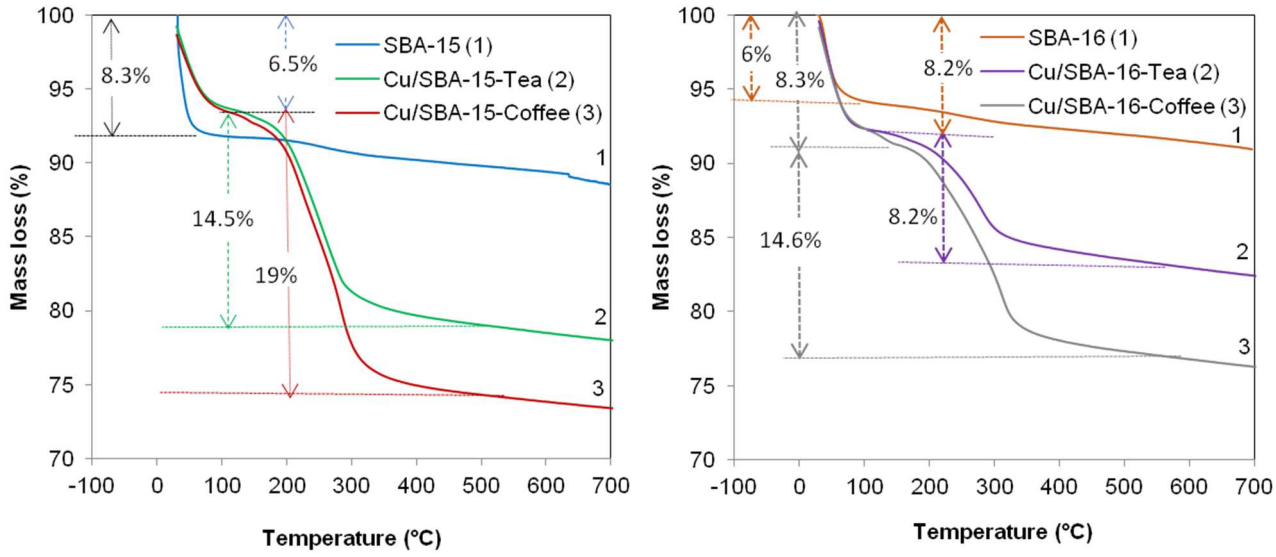


*a* *b*

**Fig. 8** TGA patterns of SBA-15 and Cu/SBA-15 (**a**) and SBA-16 and Cu/SBA-16 (**b**).

Beyond 170 °C, similar weight losses of ca 14.5 % for Cu/SBA-15-Tea and 9.3 % for Cu/SBA-16-Tea were noticed, presumably due to tea component decomposition. This result is of great importance because it allows establishing the thermal stability threshold at this temperature. Consequently, accurate assessment of the CRC and WRC can easily be achieved through repetitive TPD runs below 150 °C for Cu-loaded organo-SBA.

Higher mass losses of approximately 19 % and 14.6 %, respectively were obtained with coffee-modified counterparts. This is probably due to the incorporation of a higher amount of organic components of coffee as compared to green tea [62]. This can explain somehow the lower decay in SSA and pore volume when using green tea as a result of weaker pore obstruction and surface coverage by green tea components as compared to coffee. This phenomenon was much more visible in SBA-16 samples, and confirms the formation of organically entrapped CuNPs outside the interconnected channels.

### *3.5. Interaction on silica surface*

FTIR spectra of Coffee- (**Fig. 9a**) and Tea-treated samples (**Fig. 9b**) showed a noticeable intensity increase of the broad 3700-3100 $cm^{-1}$ band. This was attributed to the hydroxyl groups brought by the insertion of coffee and tea components. This was confirmed by marked intensity increase for the 1642 and 1384 $cm^{-1}$ bands attributed to polyphenols and N-compounds. The lower

intensity of the bands appearing at 464 $cm^{-1}$ and 1085 $cm^{-1}$ (symmetric and asymmetric Si-O-Si bond stretching), at 803 $cm^{-1}$ (Si-O stretching) and at 967 $cm^{-1}$ (Si-OH) [63] suggests the occurrence of interaction between the organic molecule and silica surface.

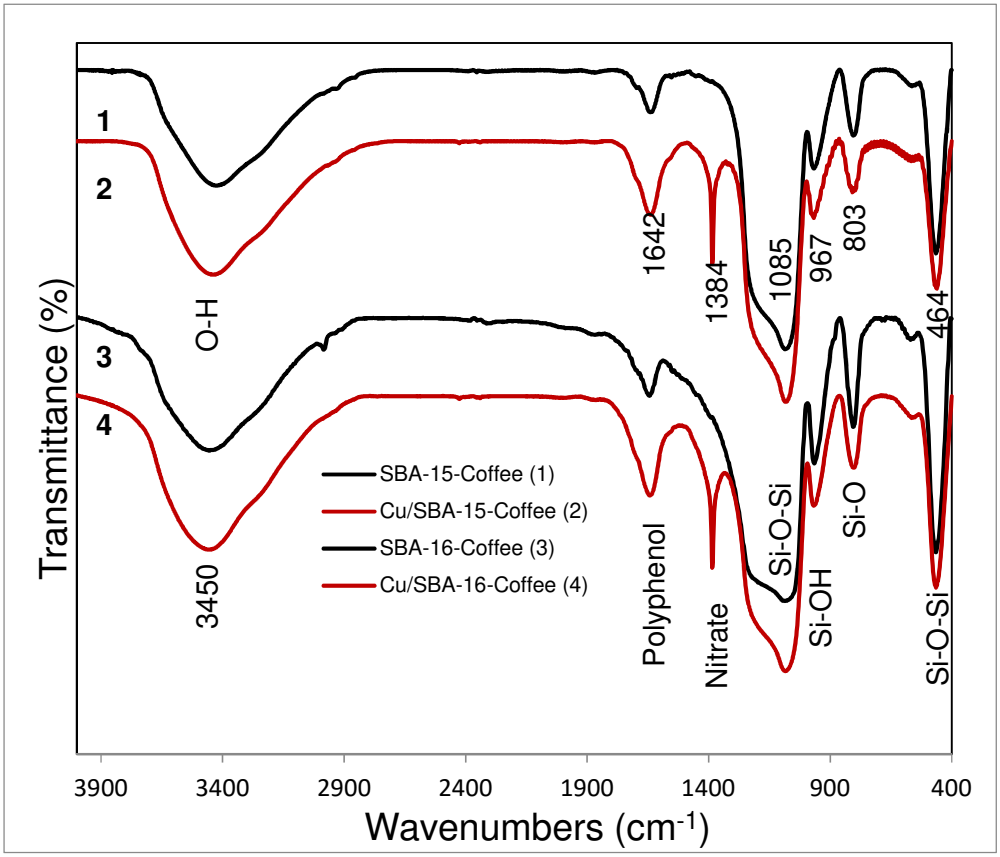


**a**

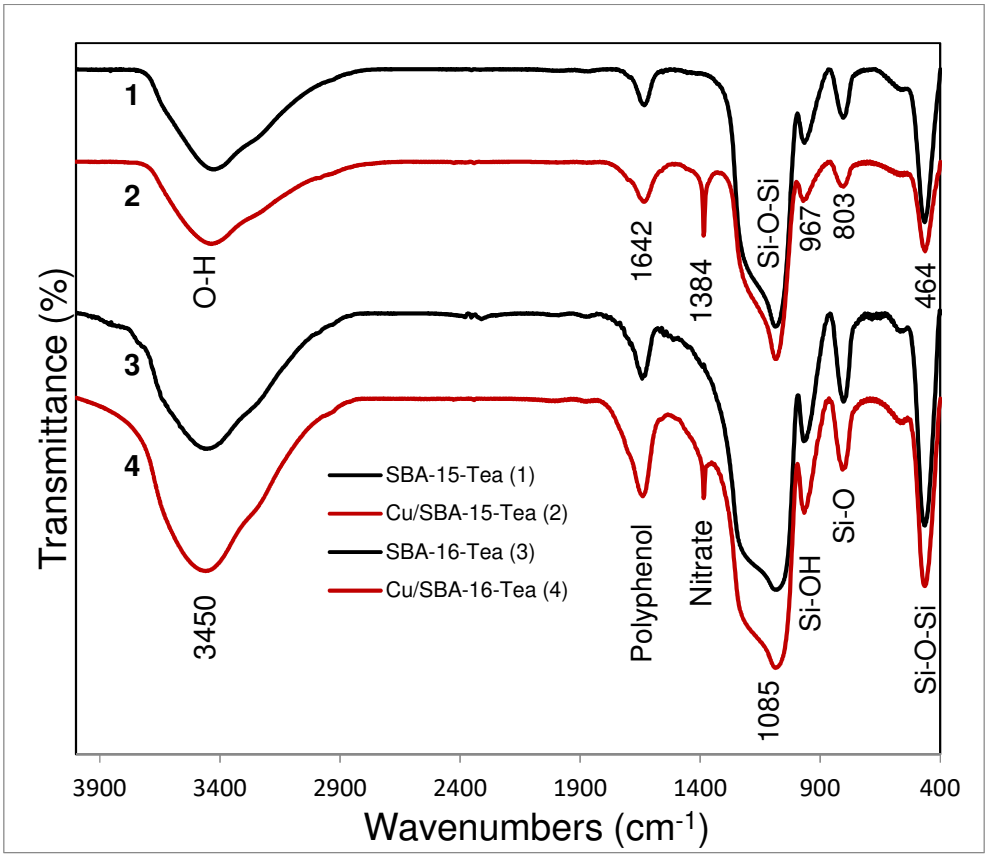


**b**

**Fig. 9** FTIR diagrams of: Coffee- (**a**) and Tea-treated SBA samples (**b**)

This result was somehow expected, given that the electron pairs of their oxygen atoms of OH, Si-O-Si and Si-OH groups should unavoidably involve Lewis-Acid-Base interaction with CuNP and H-bridges with the hydroxyl and carboxyl groups of coffee and tea components. This phenomenon appears to be more pronounced in Cu/SBA-15-Coffee as compared to Cu/SBA-16-Tea, thereby confirming the occurrence of more dispersed CuNP in less compact and more diffuse Cu-loaded organic clusters. Here, the slightly higher acidity of SBA-16 must play a certain role in providing lower Lewis basicity as compared to SBA-15. The latter is assumed to have a framework with less edge structure and, subsequently, less edge silanols and more Si-O-Si group than SBA-16. This will be examined by further TPD measurements.

### *3.6. Adsorptive properties*

The TPD technique allows evaluating the basicity and hydrophobicity of the SBA samples before and after the insertion of the copper by studying their interaction with $CO_2$. Specific $CO_2$-TPD (**Fig. 10**) and Water-TPD profiles (**Fig. 11**) were recorded for the different materials investigated herein. A quick overview of the data obtained showed a significant increase in the amounts of retained $CO_2$ and moisture after copper incorporation.

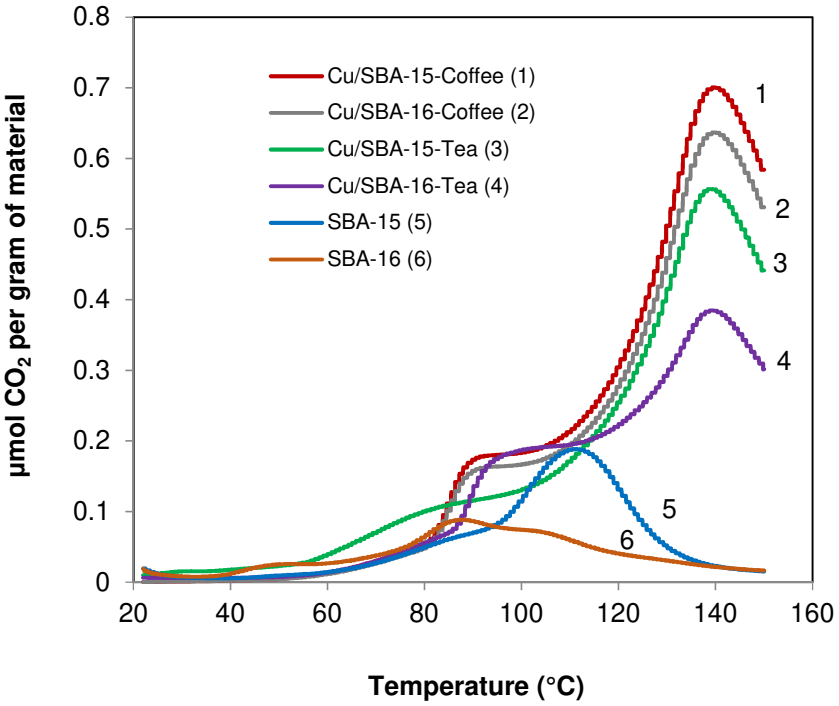


**Fig. 10** TPD patterns of $CO_2$ for SBA and CuNP-SBA samples. These purely qualitative TPD were achieved after dynamic impregnation with $CO_2$ at 20 °C under a 15 mL.min$^{-1}$ dry nitrogen stream, followed by a purge at room temperature and TPD up to 150 °C (200 mL $CO_2$ for 45–50 mg dry adsorbent). These first TPD runs cannot be repeated for the same materials, given that the decomposition of organic dispersing agents triggers at ca. 170 ºC

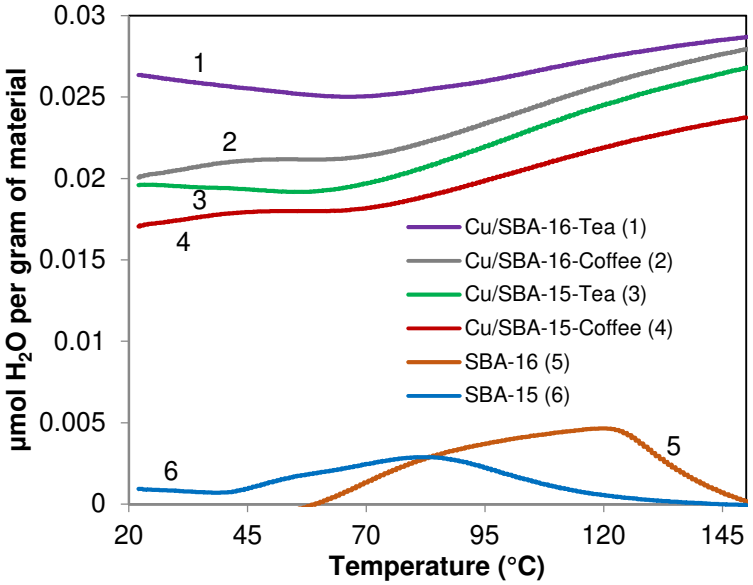


**Fig. 11** TPD patterns of water for SBA and CuNP-SBA samples. These purely qualitative TPD were achieved after dynamic impregnation with $CO_2$ at 20 °C under a 15 mL.min$^{-1}$ dry nitrogen stream, followed by a purge at room temperature and TPD up to 150 °C (200 mL $CO_2$ for 45–50 mg dry adsorbent). These first TPD runs cannot be repeated for the same materials, given that the decomposition of organic dispersing agents triggers at ca. 170 ºC

This result was somehow expected, providing clear confirmation of an increase in the number of hydroxyl groups. The latter are known to exhibit high affinity towards $CO_2$ and water. Both starting

SBA materials displayed low-intensity TPD bumps between 25 °C and 140 °C for both $CO_2$ and water. This is due to their weak surface basicity and hydrophilic character, given that pure silica is known to be rather slightly acidic materials with a low affinity towards water. The fact that all SBA-15-based materials showed higher CRC values as compared to their SBA-16 counterpart can be explained by the presence of higher amount of out-of-plane silanols (pKa 5.6) in SBA-16 due to its edge structure at channel intersection. This is known to induce higher acidity than in SBA-15 [2, 8, 13, 64].

The intensity increases and peak sharpening in $CO_2$-TPD patterns after Cu incorporation along with the noticeable shifts towards higher temperature around 135-140 °C account for an improvement of the surface basicity and an enhancement of $CO_2$ retention strength. This effect was more pronounced for Cu/SBA-15-coffee and to a lesser extent Cu/SBA-16-coffee, indicating a higher amount of newly incorporated hydroxyls. The latter are well-known to exhibit slight basicity and affinity towards Lewis acidic species like $CO_2$, metals and metal cations. This is expected to reduce the material's affinity towards water molecules, given the competitive interaction of $CO_2$ and water with hydroxyls. Conversely, relatively lower surface basicity resulted in a higher amount of retained moisture, as observed for Cu/SBA-16-Tea.

### *3.7. Correlation basicity-hydrophilic character*

Therefore, there should exist a reverse proportionality between $CO_2$ and water retention capacities (CRC and WRC, respectively) as well supported by the values assessed in the temperature range 20-150 °C (**Fig. 12**), This is due to competitive [–HO:$CO_2$], [–HO:Cu] and [–HO:$H_2O$] interactions, despite the unavoidable occurrence of water:$CO_2$ interaction in the form of carbonate-like association.

$CO_2$-TPD and $H_2O$-TPD profiles of repetitive adsorption-desorption cycles without material rehydration showed a must faster CRC decay by more than 55 % after TP2 for Cu/SBA-15-Tea, Cu/SBA-15-Coffee and Cu/SBA-16-Coffee. Less than 20 % CRC depletion was registered after TP2 and ca. 60 % after TP3 for Cu/SBA-16-Tea (**Fig. 13a**). The same tendency was observed for the WRC (**Fig. 13b**) suggesting that a part of the adsorbed $CO_2$ is due to the presence of moisture. This confirms once again the contribution of water molecules in the retention of $CO_2$. Repetitive adsorption-desorption cycles with alternate rehydration of the adsorbents gave almost similar shapes of the TPD patterns between 20-150 °C, suggesting a fully reversible $CO_2$ adsorption involving purely physical interaction, as already reported elsewhere [13, 29, 30].

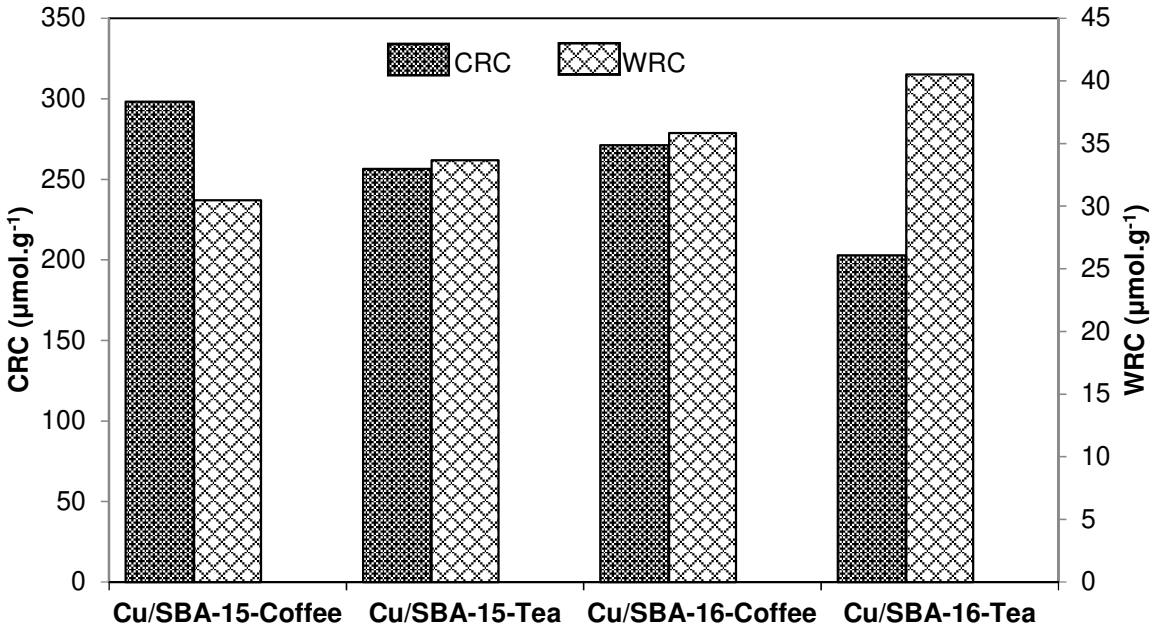


**Fig. 12** CRC versus WRC of Cu/SBA materials. These values were accurately assessed by the area of the TPD patterns between 20 °C and 150 °C. This temperature range is based on the thermal stability threshold established at 170 °C

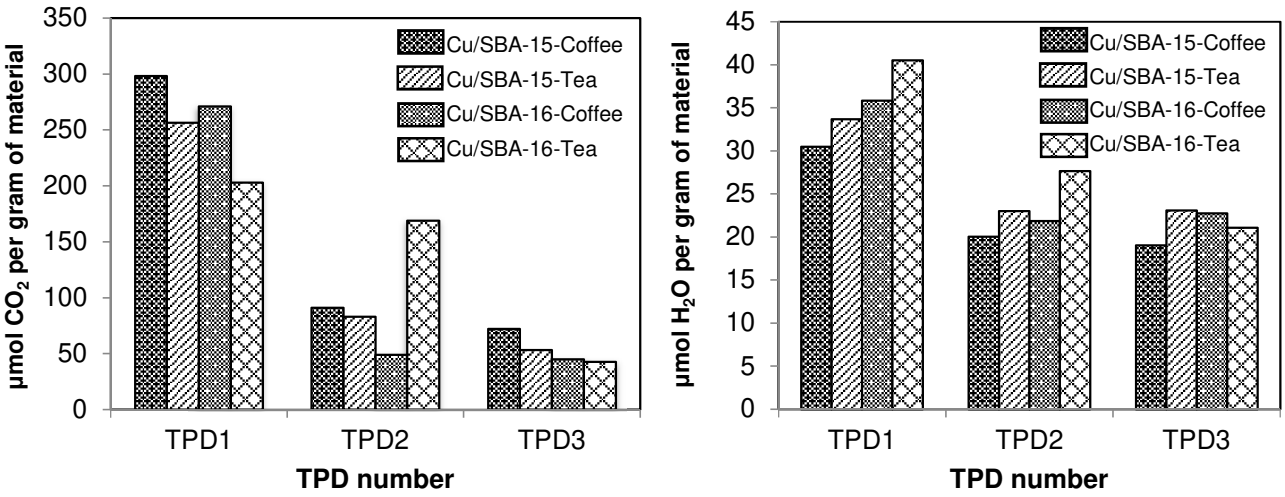


***a*** ***b***

**Fig. 13** Repetitive $CO_2$-TPD (**a**) and $H_2O$-TPD (**b**) profiles for Cu/SBA samples. These values were accurately assessed by the area of the TPD patterns between 20 °C and 150 °C. This temperature range is based on the thermal stability threshold established at 170 °C

These results are of great importance because they provide the proof of concept that CuNP incorporation induced highest basicity expressed in terms of CRC value of ca. 200-300 µmol.g$^{-1}$ and hydrophilic character in SBA-15 treated with green tea and in SBA-16 treated with coffee. Thus, it clearly appears that the beneficial role of each vegetal extract in metal dispersion is narrowly related

to the structure of the host matrix framework. These values are much higher than those reported for Cu-loaded pillared clays (170-200 $\mu mol.g^{-1}$) which displayed lower SSA [65]. Higher CRC value of ca. 1750 $\mu mol.g^{-1}$ was already reported for an MCM-48-based material displaying higher SSA but not necessarily in the same temperature range [66]. Accurate comparison with some performances reported by the literature must take into account not only the temperature range for CRC assessment but also the so-called surface affinity factor (SAF) as defined earlier [67]. Here, notwithstanding that the high SSA of SBA materials is an essential requirement for hosting highly dispersed metal nanoparticles, high SAF values can only be achieved through judiciously tailored interactions between all species present in the vicinity of adsorbent surface. These interactions are responsible for improving the surface properties. Some of them were prone to this present research, others remain to be elucidated. Investigations are still in progress in this direction.

## 4. Conclusion

The results obtained herein allow concluding that reducing agents in coffee and green tea extract produced effective copper dispersion in mesoporous SBA-like silica. Copper-loaded SBA-15 and SBA-16 showed improved surface basicity and hydrophilic character as compared to the starting materials. This effect was found to be strongly dependent on the type of reducing agent extract and silica framework. OH-compounds interactions with both copper nanoparticles and silica surface are key factor in the metal dispersion and particle size. The amount of available Si-O-Si groups appears to govern not only the metal dispersion but also the surface basicity and hydrophilic character. The findings of this research allow designing low cost and eco-friendly silica-based adsorbents for the reversible capture of $CO_2$ and moisture through optimal interactions judiciously tailored according to the desired basicity and hydrophilic character.

**Declarations**

Funding
Not applicable

Conflicts of interest
There are no conflicts to declare.

Availability of data and material
Not applicable

Code availability

Not applicable

Authors' contributions

Not applicable

Ethics approval

Not applicable

Consent to participate

Not applicable

Consent for publication

Not applicable

## References

[1] R. Ouargli, R. Hamacha, N. Benharrats, A. Boos, A. Bengueddach, β-diketone functionalized SBA-15 and SBA-16 for rapid liquid-solid extraction of copper, J. Porous Mater., 22 (2015) 511-520.
[2] R. Ouargli, S. Larouk, I. Terrab, R. Hamacha, N. Benharrats, A. Bengheddach, A. Azzouz, Intrinsic Activity of SBA-like Silica in the Catalytic Ozonation of Organic Pollutants, Ozone: Science & Engineering, 38 (2015) 48-61.
[3] Y. Ding, Q. Xian, Z. Jiang, L. Chen, T. Xiong, X. He, W. Yang, H. Dan, T. Duan, Immobilization of uranium in cristobalite ceramic through adsorption on mesoporous SBA-15 and further sintering process, Journal of the European Ceramic Society, 40 (2020) 2113-2119.
[4] T.M. Albayati, K.R. Kalash, Polycyclic aromatic hydrocarbons adsorption from wastewater using different types of prepared mesoporous materials MCM-41in batch and fixed bed column, Process Safety and Environmental Protection, 133 (2020) 124-136.
[5] D. Zhao, Q. Huo, J. Feng, B.F. Chmelka, G.D. Stucky, Nonionic Triblock and Star Diblock Copolymer and Oligomeric Surfactant Syntheses of Highly Ordered, Hydrothermally Stable, Mesoporous Silica Structures, J. Am. Chem. Soc., 120 (1998) 6024-6036.
[6] D. Zhao, Triblock Copolymer Syntheses of Mesoporous Silica with Periodic 50 to 300 Angstrom Pores, Science, 279 (1998) 548-552.
[7] G. Gonzalez, A. Sagarzazu, A. Cordova, M.E. Gomes, J. Salas, L. Contreras, K. Noris-Suarez, L. Lascano, Comparative study of two silica mesoporous materials (SBA-16 and SBA-15) modified with a hydroxyapatite layer for clindamycin controlled delivery, Microporous Mesoporous Mater., 256 (2018) 251-265.
[8] M. Sulpizi, M.-P. Gaigeot, M. Sprik, The Silica-Water Interface: How the Silanols Determine the Surface Acidity and Modulate the Water Properties, J. Chem. Theory Comput., 8 (2012) 1037-1047.
[9] L.T. Zhuravlev, The surface chemistry of amorphous silica. Zhuravlev model, Colloids Surf. Physicochem. Eng. Aspects, 173 (2000) 1-38.
[10] Y. Duval, J.A. Mielczarski, O.S. Pokrovsky, E. Mielczarski, J.J. Ehrhardt, Evidence of the Existence of Three Types of Species at the Quartz-Aqueous Solution Interface at pH 0-10: XPS Surface Group Quantification and Surface Complexation Modeling, J. Phys. Chem. B, 106 (2002) 2937-2945.
[11] O.S. Pokrovsky, S.V. Golubev, J.A. Mielczarski, Kinetic evidences of the existence of positively charged species at the quartz-aqueous solution interface, J. Colloid Interface Sci., 296 (2006) 189-194.

[12] R. Ouargli, N. Bouazizi, M. Khelil, S. Nousir, R. Benslama, S. Ammar, A. Azzouz, SBA-15-supported iron nanoparticles with improved optical properties, conductance and capacitance, Chemical Physics Letters, 673 (2017) 30-37.
[13] R. Ouargli-Saker, N. Bouazizi, B. Boukoussa, D. Barrimo, A. Paola-Nunes-Beltrao, A. Azzouz, Metal-loaded SBA-16-like silica - Correlation between basicity and affinity towards hydrogen, Appl. Surf. Sci., 411 (2017) 476-486.
[14] R. Liu, W. Cai, X. Ni, L. Shi, R. Wang, S. Lin, Ultrastable and strongly acidic Al-SBA-15 with superior activity in LDPE catalytic cracking reaction, J. Solid State Chem., 286 (2020) 121319-121319.
[15] X. Cao, L. Li, Y. Shitao, S. Liu, Y. Hailong, W. Qiong, A.J. Ragauskas, Catalytic conversion of waste cooking oils for the production of liquid hydrocarbon biofuels using in-situ coating metal oxide on {SBA}-15 as heterogeneous catalyst, J. Anal. Appl. Pyrolysis, 138 (2019) 137-144.
[16] A.A. Hussain, S. Nazir, R. Irshad, K. Tahir, M. Raza, Z.U.H. Khan, A.U. Khan, Synthesis of functionalized mesoporous Ni-SBA-16 decorated with MgO nanoparticles for Cr (VI) adsorption and an effective catalyst for hydrodechlorination of chlorobenzene, Mater. Res. Bull., 133 (2021) 111059.
[17] T. Qiang, Y. Song, J. Zhao, J. Li, Controlled incorporation homogeneous Ti-doped SBA-15 for improving methylene blue adsorption capacity, Journal of Alloys and Compounds, 770 (2019) 792-802.
[18] M. Neek, T.I. Kim, S.-W. Wang, Protein-based nanoparticles in cancer vaccine development, Nanomed. Nanotechnol. Biol. Med., 15 (2019) 164-174.
[19] G. Vares, V. Jallet, Y. Matsumoto, C. Rentier, K. Takayama, T. Sasaki, Y. Hayashi, H. Kumada, H. Sugawara, Functionalized mesoporous silica nanoparticles for innovative boron-neutron capture therapy of resistant cancers, bioRxiv, (2018).
[20] S. Ullah, A. Ahmad, A. Wang, M. Raza, A.U. Jan, K. Tahir, A.U. Rahman, Y. Qipeng, Bio-fabrication of catalytic platinum nanoparticles and their in vitro efficacy against lungs cancer cells line (A549), J. Photochem. Photobiol. B: Biol., 173 (2017) 368-375.
[21] S. Couillaud, M. Kirikova, W. Zaïdi, J.-P. Bonnet, S. Marre, C. Aymonier, J. Zhang, F. Cuevas, M. Latroche, L. Aymard, J.-L. Bobet, Supercritical fluid chemical deposition of Pd nanoparticles on magnesium-scandium alloy for hydrogen storage, J. Alloys Compd., 574 (2013) 6-12.
[22] E.J. Reardon, Capture and storage of hydrogen gas by zero-valent iron, J. Contam. Hydrol., 157 (2014) 117-124.
[23] R. Bargougui, N. Bouazizi, S. Ammar, A. Azzouz, Molybdenum-Loaded Anatase TiO2 Nanoparticles With Enhanced Optoelectronics Properties, Journal of Electronic Materials, 46 (2016) 85-91.
[24] S. Kubota, T. Morioka, M. Takesue, H. Hayashi, M. Watanabe, R.L. Smith, Continuous supercritical hydrothermal synthesis of dispersible zero-valent copper nanoparticles for ink applications in printed electronics, J. Supercrit. Fluids, 86 (2014) 33-40.
[25] K.C. Song, S.M. Lee, T.S. Park, B.S. Lee, Preparation of colloidal silver nanoparticles by chemical reduction method, Korean J. Chem. Eng., 26 (2009) 153-155.
[26] K. Zhang, J.M. Suh, J.-W. Choi, H.W. Jang, M. Shokouhimehr, R.S. Varma, Recent Advances in the Nanocatalyst-Assisted NaBH4 Reduction of Nitroaromatics in Water, ACS Omega, 4 (2019) 483-495.
[27] Z.G. Wu, M. Munoz, O. Montero, The synthesis of nickel nanoparticles by hydrazine reduction, Advanced Powder Technology, 21 (2010) 165-168.
[28] A. Guzman, J. Arroyo, L. Verde, J. Rengifo, Synthesis and Characterization of Copper Nanoparticles/Polyvinyl Chloride (Cu NPs / PVC) Nanocomposites, Procedia Mater. Sci., 9 (2015) 298-304.
[29] N. Bouazizi, R. Ouargli, S. Nousir, A. Azzouz, Copper and palladium loaded polyol dendrimer-montmorillonite composites as potential adsorbents for CO2 and H2, J. Mater. Sci.: Mater. Electron., 30 (2019) 8182-8190.
[30] N. Bouazizi, R. Ouargli, S. Nousir, R.B. Slama, A. Azzouz, Properties of SBA-15 modified by iron nanoparticles as potential hydrogen adsorbents and sensors, Journal of Physics and Chemistry of Solids, 77 (2015) 172-177.
[31] N. Bouazizi, S. Louhichi, R. Ouargli, R. Bargougui, J. Vieillard, F.L. Derf, A. Azzouz, Cu 0 -loaded SBA-15@ZnO with improved electrical properties and affinity towards hydrogen, Applied Surface Science, 404 (2017) 146-153.
[32] R. Bodo, R. Hausler, A. Azzouz, Approche multicritère pour la sélection de plantes aquatiques en vue d'une exploitation rationnelle, Rev Sci Eau, 19 (2006) 181-197.
[33] S. Sharma, S.-F. Cheng, B. Bhattacharya, S. Chakkaravarthi, Efficacy of free and encapsulated natural antioxidants in oxidative stability of edible oil: Special emphasis on nanoemulsion-based encapsulation, Trends in Food Science & Technology, 91 (2019) 305-318.
[34] S. Mukherjee, D. Chowdhury, R. Kotcherlakota, S. Patra, V. B, M.P. Bhadra, B. Sreedhar, C.R. Patra,

Potential Theranostics Application of Bio-Synthesized Silver Nanoparticles (4-in-1 System), Theranostics, 4 (2014) 316-335.
[35] R. Bodo, K. Ahmanache, R. Hausler, A. Azzouz, Optimized extraction of total proteic mass from water hyacinth dry leaves, Journal of Environmental Engineering and Science, 3 (2004) 529-536.
[36] M.R. Bindhu, V. Sathe, M. Umadevi, Synthesis, characterization and SERS activity of biosynthesized silver nanoparticles, Spectrochim. Acta, Part A, 115 (2013) 409-415.
[37] N. Ahmad, Rapid Green Synthesis Of Silver And Gold Nanoparticles Using Peels Of Punica Granatum, Adv. Mater. Lett., 3 (2012) 376-380.
[38] R. Irshad, K. Tahir, B. Li, A. Ahmad, A. R. Siddiqui, S. Nazir, Antibacterial activity of biochemically capped iron oxide nanoparticles: A view towards green chemistry, J. Photochem. Photobiol. B: Biol., 170 (2017) 241-246.
[39] M. Wang, W. Zhang, X. Zheng, P. Zhu, Antibacterial and catalytic activities of biosynthesized silver nanoparticles prepared by using an aqueous extract of green coffee bean as a reducing agent, RSC Adv., 7 (2017) 12144-12149.
[40] V.K. Vidhu, D. Philip, Catalytic degradation of organic dyes using biosynthesized silver nanoparticles, Micron, 56 (2014) 54-62.
[41] J. Venkatesan, S.-K. Kim, M. Shim, Antimicrobial, Antioxidant, and Anticancer Activities of Biosynthesized Silver Nanoparticles Using Marine Algae Ecklonia cava, Nanomaterials, 6 (2016) 235-235.
[42] W. Xu, Y. Fan, X. Liu, D. Luo, H. Liu, N. Yang, Catalytic and antibacterial properties of silver nanoparticles green biosynthesized using soluble green tea powder, Mater. Res. Express, 5 (2018) 45029-45029.
[43] A.S. Ertürk, Biosynthesis of Silver Nanoparticles Using Epilobium parviflorum Green Tea Extract: Analytical Applications to Colorimetric Detection of Hg2+ Ions and Reduction of Hazardous Organic Dyes, J. Cluster Sci., 30 (2019) 1363-1373.
[44] M. Nishibuchi, Chieng, M. Nishibuchi, Y.Y. Loo, Synthesis of silver nanoparticles by using tea leaf extract from Camellia Sinensis, Int. J. Nanomed., (2012) 4263-4263.
[45] A. Subhan, R. Irshad, S. Nazir, K. Tahir, A. Ahmad, A.U. Khan, Z.U.H. Khan, A new study of biomediated Pd/tiO2: a competitive system for Escherichia coli inhibition and radical stabilization, Mater. Res. Express, 6 (2020) 125430.
[46] Z. Yan, Y. Zhong, Y. Duan, Q. Chen, F. Li, Antioxidant mechanism of tea polyphenols and its impact on health benefits, Anim. Nutr., 6 (2020) 115-123.
[47] T. Aree, Understanding structures and thermodynamics of beta-cyclodextrin encapsulation of chlorogenic, caffeic and quinic acids: Implications for enriching antioxidant capacity and masking bitterness in coffee, Food Chem., 293 (2019) 550-560.
[48] S. Rahman, Y. Huang, L. Zhu, S. Feng, I. Khan, J. Wu, Y. Li, X. Wang, Therapeutic Role of Green Tea Polyphenols in Improving Fertility: A Review, Nutrients, 10 (2018) 834-834.
[49] S.M. Chacko, P.T. Thambi, R. Kuttan, I. Nishigaki, Beneficial effects of green tea: A literature review, Chin. Med., 5 (2010) 13.
[50] K. Yamagata, Do Coffee Polyphenols Have a Preventive Action on Metabolic Syndrome Associated Endothelial Dysfunctions? An Assessment of the Current Evidence, Antioxidants (Basel), 7 (2018) 26.
[51] S.J. Hwang, S.H. Jun, Y. Park, S.H. Cha, M. Yoon, S. Cho, H.J. Lee, Y. Park, Green synthesis of gold nanoparticles using chlorogenic acid and their enhanced performance for inflammation, Nanomedicine, 11 (2015) 1677-1688.
[52] A. Scalbert, G. Williamson, Dietary Intake and Bioavailability of Polyphenols, J Nutr, 130 (2000) 2073S--2085S.
[53] P. Kilmartin, Characterisation of polyphenols in green, oolong, and black teas, and in coffee, using cyclic voltammetry, Food Chem., 82 (2003) 501-512.
[54] A. Farah, T. de Paulis, L.C. Trugo, P.R. Martin, Effect of roasting on the formation of chlorogenic acid lactones in coffee, Journal of Agricultural and Food Chemistry, 53 (2005) 1505-1513.
[55] M. Reto, M.E. Figueira, H.M. Filipe, C.M. Almeida, Chemical composition of green tea (Camellia sinensis) infusions commercialized in Portugal, Plant foods for human nutrition, 62 (2007) 139.
[56] J. Herrera, J. Kwak, J. Hu, Y. Wang, C. Peden, J. Macht, E. Iglesia, Synthesis, characterization, and catalytic function of novel highly dispersed tungsten oxide catalysts on mesoporous silica, Journal of Catalysis, 239 (2006) 200-211.
[57] H. Sun, Q. Tang, Y. Du, X. Liu, Y. Chen, Y. Yang, Mesostructured SBA-16 with excellent hydrothermal, thermal and mechanical stabilities: Modified synthesis and its catalytic application, J. Colloid Interface Sci., 333 (2009) 317-323.

[58] K.S.W. Sing, Reporting physisorption data for gas/solid systems with special reference to the determination of surface area and porosity (Provisional), Pure Appl. Chem., 54 (1982) 2201-2218.
[59] R. Xu, W. Pang, J. Yu, Q. Huo, J. Chen, Chemistry of Zeolites and Related Porous Materials, John Wiley & Sons, Ltd, 2007.
[60] V. Meynen, P. Cool, E.F. Vansant, Verified syntheses of mesoporous materials, Microporous and Mesoporous Materials, 125 (2009) 170-223.
[61] S.-B. Zhu, Interactions of water, ions, and atoms with metal surfaces, Surface Science, 329 (1995) 276-284.
[62] A.L. Klatsky, M.A. Armstrong, G.D. Friedman, Coffee, tea, and mortality, Ann. Epidemiol., 3 (1993) 375-381.
[63] A. Hakiki, B. Boukoussa, H.H. Zahmani, R. Hamacha, N. el Houda Hadj Abdelkader, F. Bekkar, F. Bettahar, A.P. Nunes-Beltrao, S. Hacini, A. Bengueddach, A. Azzouz, Synthesis and characterization of mesoporous silica SBA-15 functionalized by mono-, di-, and tri-amine and its catalytic behavior towards Michael addition, Mater. Chem. Phys., 212 (2018) 415-425.
[64] R. Ouargli-Saker, N. Bouazizi, S. Lassouad, S. Ammar, J. Vieillard, F. Le Derf, A. Azzouz, Copper-loaded SBA-15 Silica with Improved Electron Mobility-Conductance and Capacitance Properties, J. Inorg. Organomet. Polym Mater., 30 (2020) 5108-5117.
[65] F.C.F. Marcos, J.M. Assaf, E.M. Assaf, CuFe and CuCo supported on pillared clay as catalysts for CO2 hydrogenation into value-added products in one-step, Mol. Catal., 458 (2018) 297-306.
[66] M. Bhagiyalakshmi, P. Hemalatha, M. Ganesh, M.M. Peng, H.T. Jang, Synthesis of copper exchanged heteropolyacids supported on MCM-48 and its application for CO2 adsorption, J. Ind. Eng. Chem, 17 (2011) 628-632.
[67] A. Azzouz, S. Nousir, N. Bouazizi, R. Roy, Metal-Inorganic-Organic Matrices as Efficient Sorbents for Hydrogen Storage, ChemSusChem, 8 (2015) 800-803.